Cellulose (2023) 30:8861–8881
https://doi.org/10.1007/s10570-023-05397-0

ORIGINAL RESEARCH

# Manufacturing of cellulose-based nano- and submicronparticles via different precipitation methods

**Martin Reimer · Felix Eckel · Maximilian Rothammer · Daniel Van Opdenbosch · Cordt Zollfrank**

Received: 16 December 2022 / Accepted: 12 July 2023 / Published online: 30 July 2023


**Abstract** Nanoprecipitation is one of the most popular methods for producing polymer nanoparticles. However, the reported results show a large variability. In order to provide a first-hand comparative study, we prepared cellulose-based nanoparticles via different nanoprecipitation methods. Here, the influence of the coagulating solvents acetone, *N*,*N*-dimethylacetamide and tetrahydrofuran on the size and shape of the particles via precipitation using dialysis was investigated. The influence of temperature and concentration was determined by dropwise addition of the coagulation medium. Then, via rapid solvent shifting, particles were prepared from cellulose acetates with different molecular masses and the cellulose acetate propionate and cellulose acetate butyrate derivatives in the concentration range of 1–20 mg $mL^{-1}$. Thereby, it was possible to prepare spherical particles in the range from 43 to 158 nm. Furthermore, the impact of the molecular weight of these derivatives on the obtained particle size distributions was determined. It is possible to obtain pure regenerated cellulose particles in the nanometer range by a deacetylation of the derivatives. In addition, the findings were used to directly convert cellulose from a DMAc/LiCl solvent system into regenerated cellulose nanoparticles with a size of $10 \pm 3$ nm.

**Supplementary Information** The online version contains supplementary material available at https://doi.org/10.1007/s10570-023-05397-0.

M. Reimer · F. Eckel · M. Rothammer · D. Van Opdenbosch · C. Zollfrank (✉)
Chair for Biogenic Polymers, Campus Straubing for Biotechnology and Sustainability, Technical University of Munich, Schulgasse 16, 94315 Straubing, Germany
e-mail: cordt.zollfrank@tum.de

M. Reimer
e-mail: martin.reimer@tum.de

F. Eckel
e-mail: felix.eckel@tum.de

M. Rothammer
e-mail: maximilian.rothammer@tum.de

D. Van Opdenbosch
e-mail: daniel.van-opdenbosch@tum.de

**Graphical abstract**

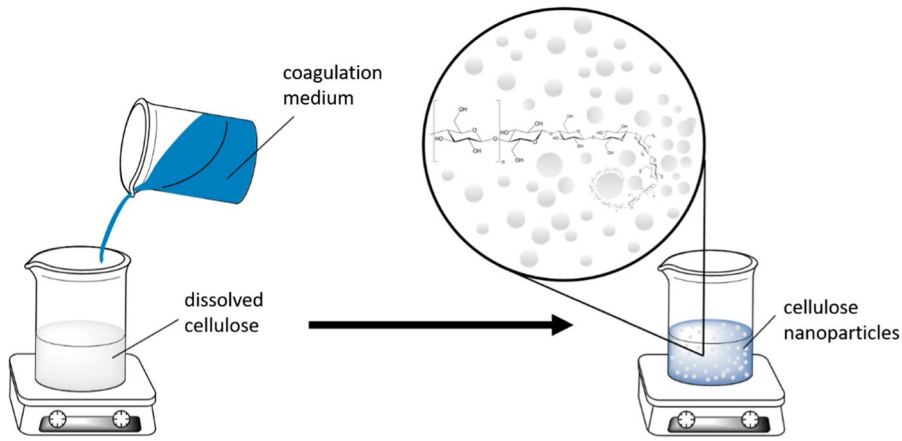


**Keywords** Cellulose · Nanoparticle · Nanoprecipitation · Solvent displacement · Solvent shifting · Interfacial deposition · Shape

## Introduction

The physicist and Nobel laureate Richard Feynman is considered the intellectual father of nanotechnology. In his famous speech from 1959 "*There's plenty of Room at the Bottom*" Feynman demonstrated the amazing possibilities of the atomic level (Feynman 1960). His inspirations would later become the basis of nanotechnology. The term "nano" typically encompasses structural dimensions in the range of 1–100 nm. In this range, materials possess unique physical properties compared to the bulk material (Zhao and Winter 2015). A variety of different structures and shapes such as nanofibers, nanofoams, nanorods and even nanosheets have been developed until now. Spherical nanoparticles (NPs) can be classified as nanocapsules and nanospheres, which differ in their internal morphology. A nanocapsule, for example, consists of a polymeric shell, whereas nanospheres are based on a continuous polymeric network (Zielińska et al. 2020).

In addition to the already established fabrication of inorganic or metallic NPs, organic biopolymers can also be converted into nanospheres. There have already been studies about particles of poly(ε-caprolactone), poly(ethylene glycol), as well as poly(lactic acid) (Zielińska et al. 2020), dextran and pullulan (Aschenbrenner et al. 2013), lignin, starch, chitosan and gelatin (Luzi et al. 2019), as well as cellulose-based polymers (Carvalho et al. 2021).

Cellulose in particular shows great potential in the field of polymer science and technology: It is the most abundant polymer on earth and is known for its low-cost, non-toxicity, environmental friendliness, biocompatibility, biodegradability, thermal and chemical stability and especially its derivatizability and is therefore used in different application fields (Wang et al. 2016; Rothammer et al. 2023). In order to combine these advantageous properties of cellulose with the application potential of NPs, a number of different fabrication options are available.

Typically, polymer NPs are generally made from solutions. In the case of cellulose, a variety of derivatizing or non-derivatizing solvent systems are available for this purpose (Rahn et al. 1996; Heinze and Koschella 2005; El-Wakil and Hassan 2008). In addition, it is also possible to specifically modify cellulose in a targeted manner, such as cellulose esters (e.g. CA) or ethers (e.g. methyl cellulose or hydroxy ethyl cellulose), which are soluble in water and common organic solvents. With these modifications, cellulose-based polymers can be readily dissolved for the subsequent processing via various methods to obtain NPs.

In general, the following processes can be applied for the production of spherical particles in the micrometer, submicrometer and nanometer range: emulsification, microfluidics, nanoprecipitation, as well as mechanical, chemical and/or enzymatic treatments as reviewed by Carvalho et al. (2021). By adjusting the process parameters, the resulting particle sizes can then be individually controlled.

The emulsion technique is a standard method for the production of spherical particles. Here, water in oil or oil in water emulsions can be used. This technique offers two main methods to obtain solid particles: On the one hand, there is the spontaneous emulsification solvent evaporation method. Here, particles with an average size between 100 and 200 nm can be produced (Szczęch and Szczepanowicz 2020). For this process, the respective polymer is dissolved in an organic solvent and carefully added to an aqueous phase with surfactants. A nanoemulsion can then be generated by high-speed homogenization or ultrasonication. Subsequent evaporation of the organic phase yields particles in the submicrometer and nanometer range. On the other hand, the emulsification and freeze-drying process can be used for particle formation (Zhang et al. 2017). Here, the polymers are dissolved in an aqueous phase and a water in oil emulsion is produced. The dispersed phase is then frozen and separated from the continuous oil phase via filtration. Subsequently, the frozen organic particle suspension can be freeze-dried to obtain porous particles.

In addition to these established methods, there are also innovations such as the premix membrane emulsification method. This process is one of the most recent developments for the fabrication of microstructured systems. Here, the premix represents a pre-emulsion and is produced by carefully mixing of two phases. These are subsequently transferred under pressure through a membrane. The transmembrane pressure and the implied shear stress cause a decrease of the droplet size. After transfer into the coagulation medium, the cellulose contained in the dispersed phase is regenerated. Via this process, cellulose particles in the size range of 160–170 nm can be obtained (Carrick et al. 2014).

The purpose of using microfluidic devices is to manipulate fluids in channels at the microscale. They have been widely used in the field of nanotechnology. In many cases, two immiscible liquids are applied. These liquids encounter each other via a T-junction (Cui et al. 2022) or a concentric glass capillary microfluidic device in a counter-flow configuration (Yeap et al. 2017). Syringe pumps can control the flow rates of both streams separately. The induced shear forces can thus be used to form monodisperse droplets. If a dissolved polymer is present in the dispersed phase, it can then be regenerated by the introduction of a coagulation medium or by evaporation. These processes can form spherical particles or also particles with other shapes.

Nanoprecipitation, also known as solvent displacement or interfacial deposition, is one of the most common methods for the preparation of particles in the submicrometer and nanometer range (Zielińska et al. 2020). Here, the polymers are dissolved in a solvent that is miscible in water. Under specific conditions, a highly diluted solution can be added dropwise to the antisolvent, or the antisolvent can be added dropwise to the solution. Due to the rapid spontaneous diffusion of the polymer solution into the aqueous phase, nanoparticles are formed. By using cellulose or cellulose derivatives, particles in the size range of 50–300 nm have already been reproducibly obtained (Carvalho et al. 2021). The influence of different processing parameters has mainly been determined empirically.

A new solvent-free approach was presented by Beaumont et al. (2016). Here, semi-crystalline and spherical cellulose-based nanoparticles were produced by reorganizing a regenerated cellulose precursor through a simple surface modification. For this purpose, TENCEL® gel, which consists of interacting particles with a well-defined fibrillary nanostructure, was transformed into spherical nanoparticles by carboxymethylation and subsequent homogenization. The repulsive anionic charges of the carboxylate groups improved the stability of the resulting colloidal suspension by preventing its aggregation. This process allowed the preparation of well-defined spherical cellulose nanoparticles with adjustable diameters of 129 nm, 107 nm and 73 nm. The particles obtained consist of a crystalline core and an amorphous, highly carboxymethylated shell. In another approach, particles with a core diameter of 16 nm and a cladding thickness of 18 nm could be detected (Beaumont et al. 2019). If these particles are stored under standard conditions, the outer shell is able to swell. When the particles are stored under

acidic conditions, their shell collapses. At a higher solids content of > 3 wt%, the various particle shells can have an interaction with each other to form a network structure. The cellulose II hydrogel can also be processed into nanoparticles by aqueous cationisation with glycidyltrimethylammonium chloride and a subsequent shearing process. These generated particles had a hydrodynamic radius of 55 nm with an intrinsic solid core and soft shell structure (Solin et al. 2020).

In addition to these established methods, there are also more rarely applied processes. For a mechanical treatment, cellulose can first be dissolved in a deep eutectic solvent such as guanidine hydrochloride and anhydrous phosphoric acid and then regenerated in ethanol (Sirviö 2019). High speed homogenization treatment followed by a microfluidizer leads to disintegration. This process can result to the formation of fibrous NPs with a diameter of about 5.6–5.8 nm and a length of tens of nanometers. For a chemical production of cellulose nanospheres, Lyocell fibers can first be treated with a 1 M NaOH solution (Yu et al. 2017). This removes possible impurities and leads to swelling of the amorphous regions. Subsequently, the treated fibers can be processed with a mixture of 90% formic acid and 10% hydrochloric acid. After neutralization, the obtained particles can be freeze-dried. Following such a chemical process, it is possible to obtain cellulose NPs with a diameter of about 27 nm. In addition, cellulose can also be selectively oxidized at the C6 position by the presence of TEMPO and at the C2 and C3 positions of the anhydroglucose unit by $NaIO_4$ (Kumari et al. 2018). This leads to the formation of a COOH group at the C6 position and to the formation of aldehyde groups at C2 and C3 positions, respectively. The resulting oxidized cellulose-based NPs have a size of smaller than 30 nm. For enzymatic treatment of cellulose, the fibers can first be swollen in a glycerol solution. This should increase the accessibility of the enzymatic hydrolysis reaction. Subsequently, spherical cellulose NPs with an average size of 30 nm can be obtained via enzymolysis by using a cellulase-xylanase complex (Chen et al. 2018). By all these different methods, it is possible to produce particles from cellulose or one of its derivatives. Depending on the choice of the appropriate system, spheres or particles in different shapes, as well as in different sizes from the micrometer to submicrometer or even nanometer range can be produced.

The particles obtained by one of these methods have a wide range of applications. One of the main applications is the use as drug delivery carrier of pharmaceuticals. Since cellulose is a biocompatible material, its use can lead to a controlled release of drugs into the human body. In addition, the spheres protect the drugs or other molecules with biological activity against the surrounding environment. These properties favor the use of a nanosuspension for the treatment of ocular diseases (Kannan et al. 2018). In addition, nanomaterials can serve as carriers for certain anticancer drugs such as docetaxel, paclitaxel, and etoposide (Raghav et al. 2021). In particular, pH-responsive drug delivery can significantly improve treatment outcomes. In this regard, cellulose-based beads, may be useful for cancer therapy, in wound healing, and in enhancing tissue regeneration (Mohan et al. 2022). Moreover, nanoparticles loaded with biocide can be used for antimicrobial surface coatings (Cordt et al. 2020).

Besides medical applications, cellulose spheres can also be used in other technical applications. By using a microfluidic device, it is possible to arrange cellulose nanocrystals into structurally colored microparticles. These can subsequently be used to fabricate photonic materials or pigments (Parker et al. 2022). In addition, spheres can also be applied as a component in semiconductor nanocomposites in electronic devices (Terna et al. 2021) and can also be useful for the development of biodegradable transistors and batteries (Zhang et al. 2019). Spheres and capsules also have a potential as carriers of antioxidants and preservatives in food packaging (Barreras-Urbina et al. 2016). The attention of nanotechnology for cellulose-based NPs is continuously increasing and its innovative use is becoming established in various sectors.

Since the empirical results on nanoprecipitation vary from approach to approach in different publications, this work focuses on a unified comparative study of the production of particles via different types of precipitation methods using a wide range of substrates. Especially simple and fast methods are demonstrated here. For this purpose, the influence of different cellulose acetate derivatives will be investigated in particular. In addition, the information obtained is used to produce the smallest possible pure cellulose NPs.

## Materials and methods

### Materials

Microcrystalline cellulose (MCC) (degree of polymerization (DP) = 221, $M_w$ = 35,800 g mol$^{-1}$) and 99% *N*,*N*-dimethylacetamide (DMAc) were purchased from Merck KGaA and Alfa Aesar (Germany), respectively. Tetrahydrofuran (THF) and lithium chloride (LiCl) were obtained from VWR (Germany). Cellulose diacetate pure granules (CDA), cellulose acetate (CA30k, $M_n$=30,000 g mol$^{-1}$), cellulose acetate (CA50k, $M_n$= 50,000 g mol$^{-1}$) and ethanol (technical, 99.6%) (EtOH) were acquired from Carl Roth GmbH & Co. KG (Germany). Cellulose acetate propionate (CAP, $M_n$ = 15,000 g mol$^{-1}$) with 0.0−1.0 wt% acetyl, 5 wt% hydroxyl, and 40−45 wt% propionyl content and cellulose acetate butyrate (CAB, $M_n$ = 12,000 g mol$^{-1}$) with 16−19 wt% acetyl and 30−35 wt% butyryl content were purchased from Sigma-Aldrich (Germany). All chemicals were used as received without further purification.

### Precipitation via dialysis

For the precipitation via dialysis, 0.1 g of cellulose acetate ($M_n$= 30,000 g mol$^{-1}$) was dissolved in 10 mL of acetone, DMAc, or THF, respectively. The solutions were each transferred into a dialysis tube with a molecular weight cut-off (MWCO) of 3,500 Da and washed five times for 3 h in each case against water. The procedure was carried out at room temperature (RT).

### Particle formation via solvent displacement

For the preparation of particles via a solvent displacement process, CDA was dissolved in 50 mL THF to obtain different concentrations of 1, 5, 10, 15 and 20 mg mL$^{-1}$. The solutions were kept at RT or were cooled with an ice bath (IB). At a stirring speed of 350 rpm, 100 mL distilled water were added dropwise via a syringe pump with a flow rate of 10 mL min$^{-1}$. THF was then removed in a water bath at 73 °C. The obtained aqueous suspensions were then filtered through a 5.0 µm syringe filter to remove macroscopic agglomerates.

### Particle formation via rapid solvent shifting

For the production of particles via the rapid solvent shifting process, various cellulose acetate types with different chain lengths CA30k, CA50k and CDA as well as CAP and CAB were each dissolved in 50 ml THF to acquire different concentrations of 1, 5, 10, 15 and 20 mg mL$^{-1}$. Subsequently, the solutions were cooled in an IB. With a stirring speed of 350 rpm, 100 ml of distilled water was then added in one single batch. THF was then removed in a water bath at 73 °C. The obtained aqueous suspensions were then filtered through a 5.0 µm syringe filter to remove macroscopic agglomerates.

### Fabrication of regenerated cellulose nano- and submicroparticles

Two approaches were pursued for the production of regenerated cellulose NPs: (1) the deacetylation of cellulose acetate derivative NPs and (2) the dissolution and precipitation of MCC via rapid solvent shifting.

(1) For the deacetylation, 10 mg of the CAP spheres were suspended in 1.5 mL of a 0.15 M NaOH solution in 96 vol% ethanol and stirred for 24 h at RT. The dispersion was then transferred to a dialysis tube (MWCO 3,500 Da) and washed five times against water for 3 h in each case.

(2) MCC was dissolved in DMAc/LiCl according to our previous publication (Reimer et al. 2021). In brief, 5 g of MCC (30.9 mmol) was freeze-dried and then suspended in 100 mL of DMAc. The mixture was equipped with a calcium chloride drying tube and stirred for 72 h at RT. 9.81 g LiCl (231.4 mmol) was dried in an oven at 105 °C. The cellulose suspension was slowly heated to 90 °C and stirred for 1 h at this temperature. The dry LiCl was finely ground with pestle and mortar and slowly added to the cellulose suspension. The batch was then cooled by 0.53 °C per minute to RT. Subsequently, 2 mL was taken from this solution and diluted with 48 mL of DMAc. The diluted solution was then cooled in an IB. At a stirring speed of 350 rpm, 100 mL of distilled water was added at once. The obtained white dispersion was then transferred to a dialysis tube (MWCO of 3,500 Da) and washed five times against water for a period of 3 h each to remove DMAc and LiCl. The cloudy

dispersions obtained were used for transmission electron microscope (TEM) imaging.

### Infrared spectroscopy

For the evaluation of the deacetylation of CAP nanoparticles, Fourier transform infrared (FTIR) spectra were recorded from dried particles. The characterization was performed using a Frontier MIR spectrometer (L1280018) with an attenuated total reflection (ATR) diamond (PerkinElmer, Germany). All spectra were obtained from 8 scans with a resolution of 4 $cm^{-1}$ and in the ATR mode using a wavenumber range from 400 to 4000 $cm^{-1}$.

#### *Elemental analysis*

To evaluate the degree of substitution (DS), the elemental composition of the different cellulose acetate derivatives was measured by a Euro EA-Elemental Analyser (Eurovector, Italy). 1–3 mg powder was analysed in tin crucibles.

#### *Size exclusion chromatography (SEC)*

The molecular weight of the cellulose acetate derivatives was analysed by SEC in dimethylsulfoxide at 50 °C with a sample concentration of 5 g $L^{-1}$. Commercial raw polymer materials were prepared in triplicate vials whereas the fabricated nanoparticles were injected in triplicates from the same vial. The PSS SECcurity GPC system (pump PSS SECcurity, refractive index detector PSS SECcurity RI, columns AppliChrom ABOA DMSO-Phil-P-300, PSS GRAM 30 A and PSS GRAM 1000 A) was adjusted to an eluent flow rate of 0.4 mL $min^{-1}$. Molecular weights were obtained using a pullulan calibration from a molar mass at the peak maximum ($M_p$) of 342 g $mol^{-1}$ to 708,000 g $mol^{-1}$.

### X-ray diffraction

X-ray powder diffraction (XRD) was used to determine crystallite sizes and fractions of crystallinity. The data used in this work was obtained from a Bragg-Brentano powder diffractometer (Miniflex, Rigaku, Tokyo, Japan) with a copper anode, and a silicon strip detector (D/teX Ultra, Rigaku). The setup in detail: goniometer radius 150 mm; both Soller slits 2.5°; divergence slit fixed at 0.625°, but closing variably below 10° 2θ; variable anti-scatter screen; no monochromator; Kβ filter 0.06 mm nickel foil; effective receiving slit of the multiline detector 0.1 mm.

The samples were measured in low-background monocrystalline silicon holders, which were rotated during measurements to reduce the effects of preferred in-plane orientation. The data was corrected for incoherent scattering from the holders by subtraction of a blank measurement.

The data was evaluated by Rietveld refinement (BGMN, Bergmann et al., 1998), considering the machine line function, as verified by refining NIST Standards 640e and 660c (silicon and lanthanum hexaboride for peak shapes and positions). The scattering angle range $7° < 2\theta < 60°$ was considered, and the sample offset from the goniometer axis refined.

All incoherent scattering was modeled using the sum of a polynomial function and a diffractogram obtained from amorphous cellulose, after confirming its agreement with those reported in the literature (Yao et al., 2020), and using the coefficients and scaling as fitting parameters.

We modeled all coherent scattering based on the structure of cellulose II, as published by French (French 2014). Here, the molecular chains run along the unit cell direction <001>. The refinement parameters were the averaged crystallite sizes, the lattice parameters (±2%) and a single isotropic thermal diffuse scattering factor.

The recorded elastically scattered intensities were thus fully deconvolved into coherent and incoherent scattering from the samples. These were used to determine the fractions of crystallinity by the method of Ruland and Vonk (Ruland 1961; Vonk 1973).

### Scanning electron microscopy and particle size determination

SEM was performed using a DSM 940 A (Zeiss, Germany). The prepared samples were mounted on aluminum holders with carbon adhesive discs. The samples were then sputter-coated with gold/palladium. SEM images were recorded using 30 keV electron energy for cellulose acetate derivative particles and 5 keV electron energy for cellulose

particles using the secondary electron detector. The particle sizes were determined from the obtained SEM images using the ImageJ program. For this purpose, the diameters of a total of 100 particles per sample were determined individually.

### Transmission electron microscopy and particle size determination

TEM was performed at an acceleration voltage of 5 kV using a LVEM5 (Delong Instuments, Czech Republic, Brünn). Cellulose nanoparticles were suspended in EtOH and deposited on an ultrathin carbon film supported by a lacey carbon mesh on a 300 mesh gold grid (Ted Pella, USA). Particle sizes were determined from the collected TEM images using the ImageJ program. For this purpose, spherical shapes were assumed and the diameters of a total of 500 particles per sample were determined by analyzing the particle areas.

### Ubbelohde viscosity measurements

The flow times of CDA in THF in the concentration range between 0 and 15 mg $mL^{-1}$ were measured by using an Ubbelohde viscometer with type and capillary no.: 50,103/0c from the company SI Analytics GmbH (Germany, Mainz). In addition, a thermostat of the device type ME-31 A and a cooling spiral of the type ME-16G of the company Julabo GmbH (Germany, Seelbach) were used. The temperature of the water tank was $20 \pm 0.1$ °C. Before each measurement, the viscometer was rinsed three times with the sample to be analyzed and thermally equilibrated in the water tank for 10 min. Each batch was measured three times.

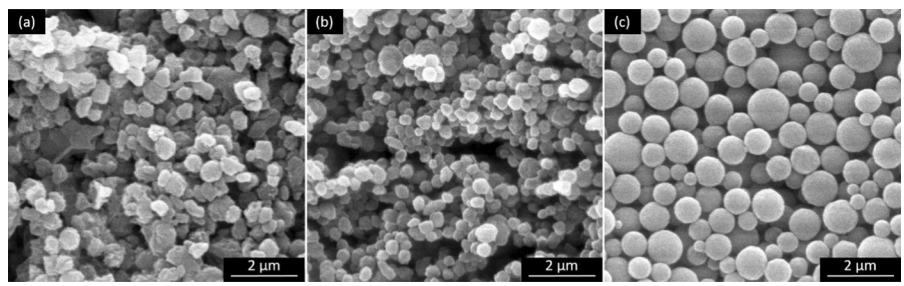


**Fig. 1** SEM images of CA30k particles produced by precipitation via dialysis. CA30k dissolved in **a** acetone, **b** DMAc and **c** THF and subsequently precipitated via dialysis against water

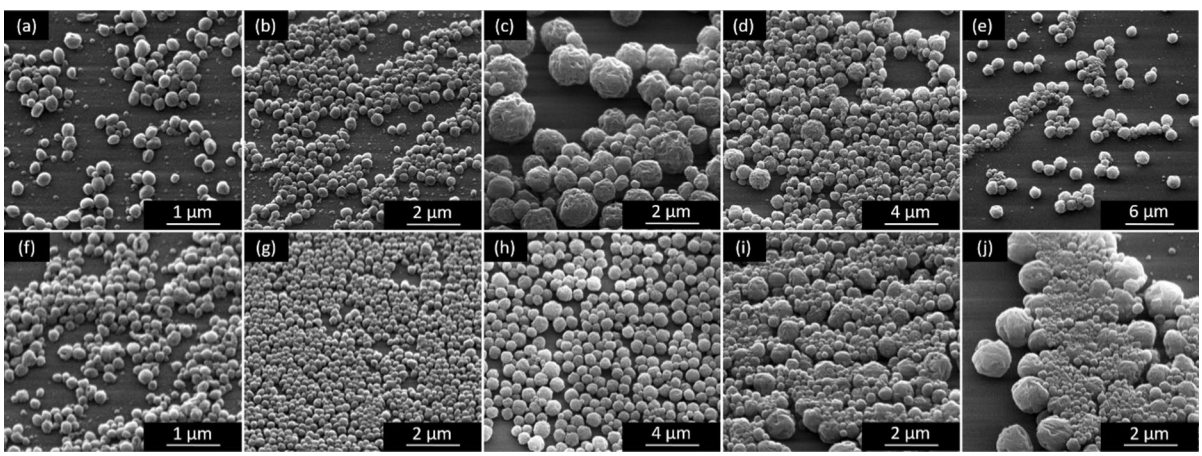


**Fig. 2** SEM images of CDA particles produced through solvent displacement method by adding the coagulation medium dropwise into the CDA solution. Uncooled with a previous concentration of CDA in THF of **a** 1 mg $mL^{-1}$, **b** 5 mg $mL^{-1}$, **c** 10 mg $mL^{-1}$, **d** 15 mg $mL^{-1}$ and **e** 20 mg $mL^{-1}$. As well as cooled with a previous concentration of CDA in THF of **f** 1 mg $mL^{-1}$, **g** 5 mg $mL^{-1}$, **h** 10 mg $mL^{-1}$, **i** 15 mg $mL^{-1}$ and **j** 20 mg $mL^{-1}$

## Results

### Precipitation via dialysis

Particles prepared via dialysis differ in terms of particle size and shape, depending on the solvent system used. All particle size distributions generated by this method exhibit a unimodal normal size distribution, Supplementary information Figure S1-S3. If the cellulose acetate CA30k was previously dissolved in acetone, the particles have an average particle diameter of $461 \pm 142$ nm. The shape of these particles in the submicrometer range is irregular and slightly sharp-edged, see Fig. 1a. CA30k particles resulting from a DMAc solution have a mean particle diameter of $352 \pm 134$ nm. The shapes of the particles also range from spherical to irregular, Fig. 1b. The particles obtained from THF have the largest dimensions with an average diameter of $590 \pm 257$ nm, but at the same time, these particles exhibit a smooth spherical shape, Fig. 1c.

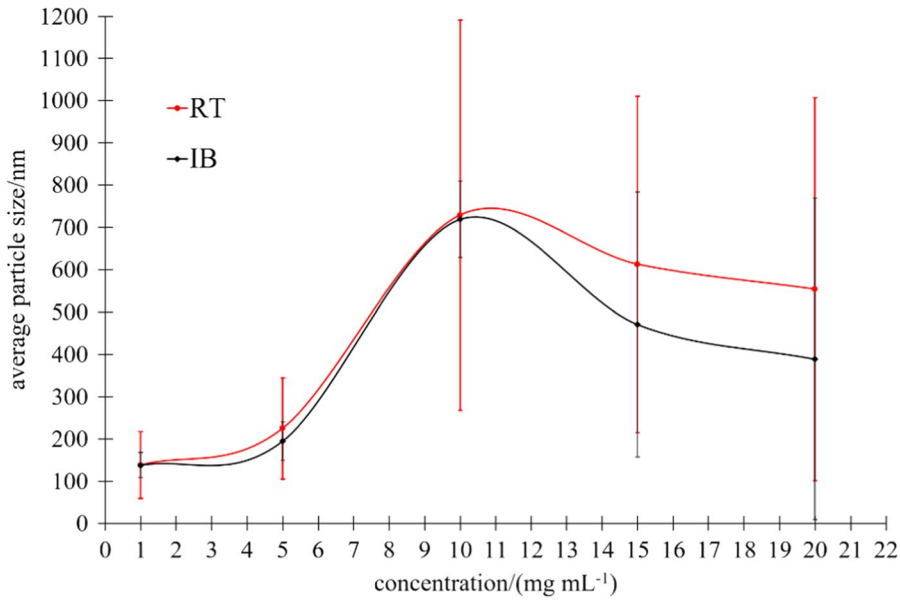


**Fig. 3** Average particle sizes in nm with standard deviation of the spheres produced via solvent displacement method at RT or cooled in an IB.

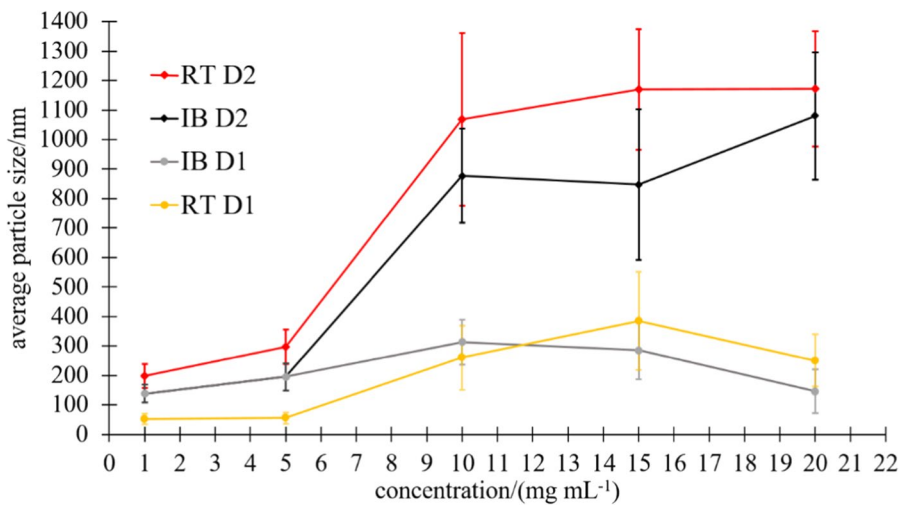


**Fig. 4** Average particle sizes in nm with standard deviation of the solvent displacement process with the different process types uncooled at RT and cooled with an IB at different concentrations of 1, 5, 10, 15 and 20 mg $mL^{-1}$. The bimodal size distributions are separated in distribution 1 (D1) and distribution 2 (D2) for smaller and bigger particle fractions, respectively

Particle formation via solvent displacement

The fabrication of particles in the nanometer and submicrometer range via the solvent displacement method produces spherical to tangle-shaped particles, either when cooled or uncooled. If the process is carried out without cooling in an IB at RT, particles with a bimodal size distribution are formed from the solutions with the concentrations of 1, 5, 10, 15 and 20 mg $mL^{-1}$, see Fig. 2 and Supplementary information Figure S4-S8. As the concentration increases, the particle diameters increase causing the size distributions to shift to the micrometer range.

If the entire particle size distribution is considered, the average particle diameter in the concentration range of 1, 5 and 10 g $mL^{-1}$ increases from $138 \pm 79$ nm to $225 \pm 120$ nm and $729 \pm 462$ nm, respectively, Fig. 3. When the concentration of the solution for the solvent displacement method is further increased, the mean particle diameter for the entire sample changed to $613 \pm 398$ nm for 15 mg $mL^{-1}$ and $554 \pm 453$ nm for 20 mg $mL^{-1}$.

If the solvent displacement method is carried out under cooling with an IB, a normal unimodal size distribution is achieved at concentrations of 1 and 5 mg $mL^{-1}$. When the concentration is further increased, a bimodal distribution is formed here as well, see Supplementary Figure S9-S13. At concentrations of 1, 5 and 10 mg $mL^{-1}$ the average particle sizes increase from $138 \pm 30$ nm to $195 \pm 46$ nm, and $719 \pm 290$ nm, respectively. When a concentration of 15 mg $mL^{-1}$ and 20 mg $mL^{-1}$ is used, the average particle diameters decreases to $471 \pm 313$ nm and $389 \pm 380$ nm, accordingly.

Considering the obtained distributions in more detail, the bimodal size distributions can be separated and treated as distribution 1 (D1) for the distribution with the smallest particles fraction and distribution 2 (D2) for the distribution of the larger particles fraction, if available, Fig. 4. Thus, it is possible to acquire batch fragments with different particle diameters

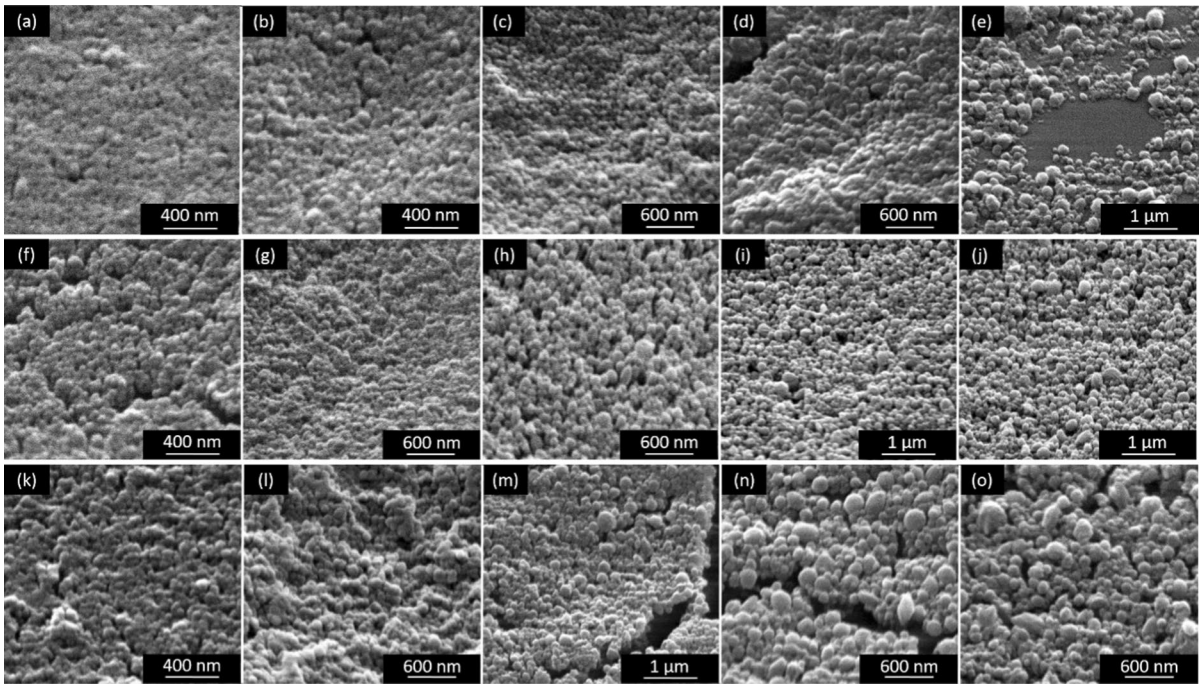


**Fig. 5** Scanning electron microscope images of cellulose acetate particles. **a**–**e** Images of CDA particles. Each fabricated with a concentration of **a** 1 mg $mL^{-1}$, **b** 5 mg $mL^{-1}$, **c** 10 mg $mL^{-1}$, **d**15 mg $mL^{-1}$ and **e** 20 mg $mL^{-1}$. **f**–**j** Images of CA30k particles. Particles are produced with a concentration of **f** 1 mg $mL^{-1}$, **g** 5 mg $mL^{-1}$, **h** 10 mg $mL^{-1}$, **i** 15 mg $mL^{-1}$ and **j** 20 mg $mL^{-1}$. **k**–**o** Images of CA50k particles. Fabricated with a concentration of **k** 1 mg $mL^{-1}$, **l** 5 mg $mL^{-1}$, **m** 10 mg $mL^{-1}$, **n** 15 mg $mL^{-1}$ and **o** 20 mg $mL^{-1}$, respectively

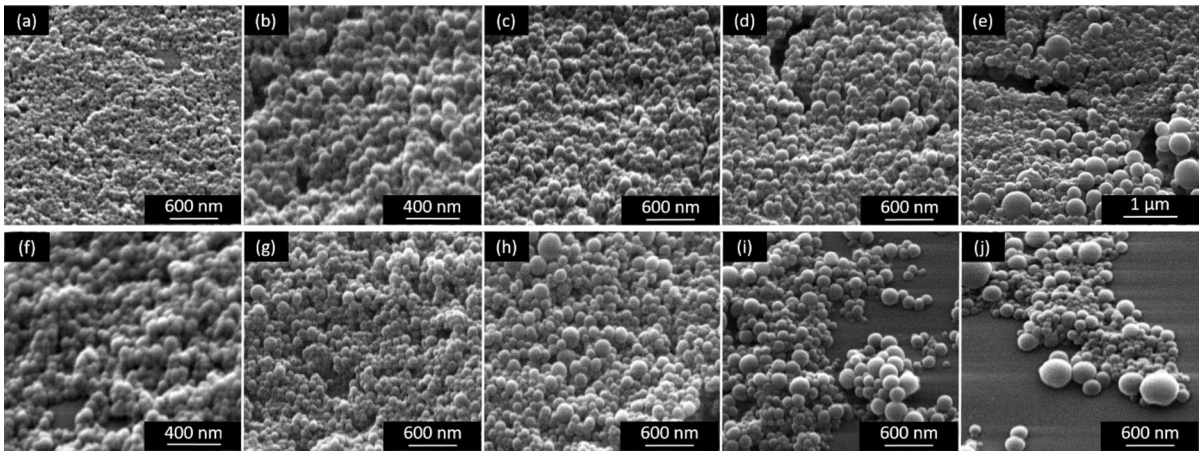


**Fig. 6** Scanning electron microscope images of cellulose acetate derivative particles. **a–e** Images of CAP spheres. Each fabricated with a concentration of **a** 1 mg $mL^{-1}$, **b** 5 mg $mL^{-1}$, **c** 10 mg $mL^{-1}$, **d** 15 mg $mL^{-1}$ and **e** 20 mg $mL^{-1}$, respectively. **f–j** Images of CAB spheres. Particles are produced with a concentration of **f** 1 mg $mL^{-1}$, **g** 5 mg $mL^{-1}$, **h** 10 mg $mL^{-1}$, **i** 15 mg $mL^{-1}$ and **j** 20 mg $mL^{-1}$

from one batch through centrifugation or filtration processes.

Particle formation via rapid solvent shifting

Particles with average diameters between 43 and 158 nm could be produced through the rapid solvent shifting using the various cellulose acetate variants in the concentration range between 1 and 20 mg $mL^{-1}$. All particles exhibited a predominantly spherical and smooth shape, see Figs. 5 and 6. Only CDA, CA30k and CA50k produced isolated irregular particle shapes at the concentrations of 15 and 20 mg $mL^{-1}$, while the majority were spherical. The size distributions of the prepared CDA particles are shown in Supplementary Figure S14-S18.

**Table 1** Average particle sizes in nm and standard deviations of the particles produced via rapid solvent shifting in the concentration range of 1, 5, 10, 15, and 20 mg $mL^{-1}$ for cellulose acetate derivatives

| Concentration/(mg $mL^{-1}$) | | | | | |
|---|---|---|---|---|---|
| Substance | 1 | 5 | 10 | 15 | 20 |
| CA30k | 43 ± 8 | 55 ± 12 | 76 ± 19 | 85 ± 21 | 134 ± 35 |
| CDA | 52 ± 8 | 63 ± 10 | 82 ± 19 | 97 ± 27 | 134 ± 54 |
| CA50k | 45 ± 11 | 77 ± 18 | 104 ± 30 | 122 ± 37 | 158 ± 84 |
| CAP | 52 ± 10 | 89 ± 20 | 103 ± 36 | 118 ± 39 | 135 ± 58 |
| CAB | 62 ± 15 | 84 ± 16 | 118 ± 48 | 135 ± 70 | 156 ± 84 |

In addition, the particle size determination of the nanoprecipitation is shown in Supplementary Figure S19-S23 for CA30k and Supplementary Figure S24-S28 for using CA50k. By using CAP or CAB as starting material, spherical shapes were always obtained over the entire concentration range.

The particles for both CAP and CAB also exhibit unimodal size distributions for the entire concentration series, see Supplementary Figure S29-S33 for CAP and S34-S38 for CAB. The mean particle sizes of the different cellulose acetate derivatives as well as the standard deviation are shown in Table 1.

Elemental analysis was used to obtain then the DS of the used cellulose acetates with different molecular weights. Here, a DS of 2.0 for CDA and a DS of 2.2 for CA30k and CA50k were determined. The data of the molecular weight distributions determined via SEC can be found in the Supplementary information Table ST1. $M_w$ of CAP was reduced by 5200 g $mol^{-1}$ and $M_n$ was reduced by 450 g $mol^{-1}$ during particle fabrication.

Fabrication of cellulose nano- and submicronparticles

Spherical nanoparticles were also generated by deacetylation of the CAP nanoparticles (method 1) and by manufacturing cellulose particles directly from a cellulose solution using the rapid solvent shifting method (method 2), Fig. 7.

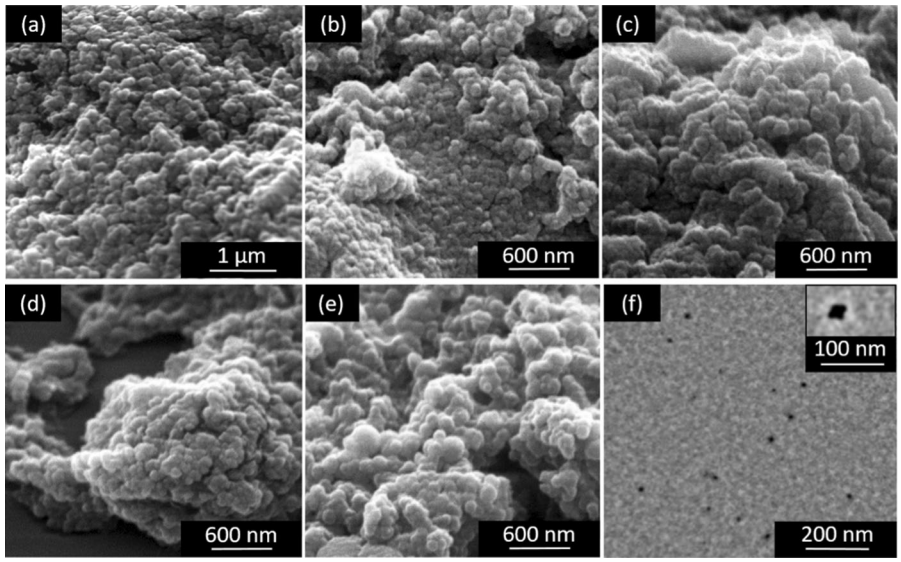


**Fig. 7** Scanning electron microscope images of cellulose nanoparticles produced via method (1) with a concentration of **a** 1 mg $mL^{-1}$, **b** 5 mg $mL^{-1}$, **c** 10 mg $mL^{-1}$, **d** 15 mg $mL^{-1}$ and **e** 20 mg $mL^{-1}$. **f** shows a transmission electron microscope image of cellulose nanoparticles fabricated through method (2). The insert shows a cluster of 4 spherical cellulose particles

The particles obtained by method (1) have a unimodal size distribution, see Supplementary Figure S39-S43. After deacetylation, the spheres have a mean particle size of $47 \pm 10$ nm, $77 \pm 11$ nm, $93 \pm 23$ nm, $102 \pm 30$ nm and $120 \pm 30$ nm for the concentrations of 1, 5, 10, 15 and 20 mg $mL^{-1}$ of CAP solution used in the precipitation process. The cellulose particles fabricated via method 2 exhibit sizes from 7 to 19 nm with a mean particle size of $10 \pm 3$ nm, Fig. 7f.

## Discussion

### Precipitation via dialysis

Precipitation via dialysis is a simple and versatile osmosis-based method for the production of particles in the nano- and submicrometer range. Here, a slow but steady solvent displacement occurs due to slow diffusion through the dialysis membrane. The solvents used (acetone, DMAc, THF) are miscible with the antisolvent and are gradually displaced by the water. The resulting solvent/antisolvent mixture is thus progressively less able to keep the polymer in solution. The additional increase in interfacial tension leads to aggregation and precipitation of the macromolecules. This results in nucleation and growth of the particles (Chronopoulou et al. 2009; Wondraczek et al. 2013). The resulting spherical shape leads to a minimization of the energy in the system. The shape as well as the size of the resulting particles can generally be influenced by the polymer concentration, temperature, the polarities of the solvent and antisolvent used and the MWCO of the dialysis membrane. In this context, it is found that both a low concentration and a low temperature leads to the formation of smaller particles. The influence of the solvent/antisolvent combination has in turn an effect on the structural morphology as well as the size. The MWCO of the dialysis tube affects the solvent mixing rate. Decreasing the MWCO will also decrease the mixing rate. This subsequently favors thermodynamic factors rather than the kinetic ones and therefore decreases the mean particle size. In this case, all parameters except the selected solvent system remained constant, so the resulting change shown in Fig. 1 is caused by the influence of the solvent/antisolvent pair.

It can be seen here that the smallest particles are produced by using DMAc as a solvent. If acetone or THF is used as an alternative solvent, the mean particle diameter increases accordingly. This observation between DMAc and acetone was also reported by Hornig and Heinze (2008).

To describe this, a correlation of size and shape to the difference in dielectric constants $\Delta\varepsilon$ of the solvent and antisolvent pair can be found (Chronopoulou et al. 2009). These differences depend on the solvent/antisolvent choice of acetone/$H_2O$ ($\Delta\varepsilon = 59.3$), DMAc/$H_2O$ ($\Delta\varepsilon = 42.3$) and THF/$H_2O$ ($\Delta\varepsilon = 72.48$)

(Bakshi et al. 1996; Chronopoulou et al. 2009). For cellulose acetate, it can be observed that the mean particle size also increases with inceasing $\Delta\varepsilon$. If THF is applied as a solvent, smooth spherical particles are preferably formed. This suggests that a high $\Delta\varepsilon$ favors a spherical morphology for cellulose acetate. In order to produce more uniform and preferably spherical particles, only THF was used as a solvent for all further experiments.

Particle formation via solvent displacement

Precipitation of nano- and submicroparticles via the solvent displacement method by a dropwise addition of the antisolvent is an alternative method for producing nanoscale particles. This process could also be carried out with DMAc, acetone or other solvents that are also miscible with water. It is preferable to select a solvent system that can be completely removed from the aqueous dispersion by evaporation. Compared to dialysis, this makes it possible to carry out the entire process in a shorter time with a greater yield. In general, the process can be executed in two ways. Either the polymer solution can be added dropwise to the antisolvent or the antisolvent can be added dropwise to the solution. According to Hornig and Heinze (2008), adding the polymer solution to the antisolvent can result in smaller particles with a broader distribution, as well as an increased amount of larger aggregates, which correspondingly reduce the yield. If the antisolvent is added to the polymer solution accordingly, larger particles with a more narrow size distribution are obtained.

Through the slow addition of the antisolvent, a slow displacement of the solvent from the polymer solution occurs, similar to the dialysis process. These concentration fluctuations then lead to the deposition of the polymer at the interface (Fessi et al. 1989). The particle formation can be explained by interface turbulence involving flow, diffusion and surface processes. These interfacial turbulences take place at non-equilibrium liquid phases of the solvent and the antisolvent and could be described by the Marangoni effect, which explains mass transport along an interface between two phases (Sternling and Scriven 1959; Fessi et al. 1989; Kannan et al. 2018). However, this complex mechanism is not completely understood and is usually explained only in terms of nucleation and growth as well as aggregation steps. The influence on the particle size is mostly characterized empirically by adjusting the process parameters (Zhao and Winter 2015; Schulze 2016; Cordt et al. 2020).

For this reason, both the influence of the polymer concentration and the influence of the temperature on the particle size distributions are investigated by using the solvent displacement method. In general, this method leads to a continuous increase in the mean particle diameter with increasing concentration (Hornig and Heinze 2008; Wondraczek et al. 2013; Schulze 2016). Here, the particle diameter also increases with increasing concentration from 1 mg $mL^{-1}$ to 10 mg $mL^{-1}$, both under uncooled and cooled conditions. In contrast to the known literature, the particle size then decreases slightly with increasing concentration. Whether cooled or not, the particle sizes are almost identical, with the exception for concentrations between 15 and 20 mg $mL^{-1}$. Only the standard deviation is smaller with cooling, Fig. 3. However, since a bimodal distribution occurs in the most cases, the two distributions must be separated and treated individually for a detailed analysis, Fig. 4.

This shows that with increase in concentration, the fraction of larger particles is favored in D2. This is also consistent with the mechanisms of nucleation, as well as growth and aggregation processes: With increasing concentration, the possibility of more macromolecules attaching to the initial nuclei from the solution or of multiple nuclei aggregating increases. This results in an increase of the average particle diameter (Schulze 2016). Nevertheless, the behavior of the smaller fraction D1 is different. Here, an increase and a decrease of the particle size in dependence of the concentration can be clearly seen.

A similar trend is also observed, when the entire process runs at low temperatures. Here, however, unimodal size distributions occur at low concentrations of 1 and 5 mg $mL^{-1}$. For 1 mg $mL^{-1}$ ($138 \pm 30$ nm), this unimodal distribution corresponds exactly to the mean value from the process at RT when the batch is considered in its entirety. At 5 mg $mL^{-1}$, the particle size of $195 \pm 46$ nm is slightly smaller than the entirety of the distribution at RT. For 10, 15, and 20 mg $mL^{-1}$, a bimodal distribution is also observed in the cooled processes. In

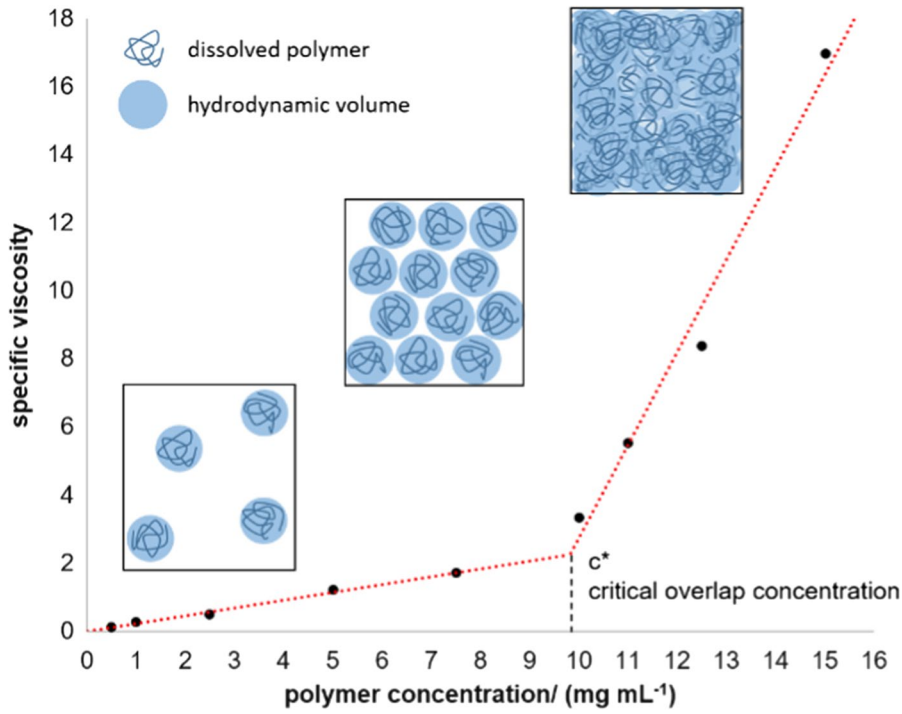


**Fig. 8** Determination of the critical overlap concentration (c*) by viscosity measurements of CDA in THF in the concentration range of 0–15 mg $mL^{-1}$

general, the size of the D1 fraction reaches its maximum at 10 mg $mL^{-1}$ and then decreases again. However, the D2 fraction generally tends to increase, but is always below the values of the D2 fraction without cooling. From this, it can be concluded that cooling has an effect on nucleation, nucleus growth and aggregation of nuclei and favors the formation of a higher proportion of smaller and more uniform particles. This is consistent with the current theory on particle nucleation and growth (Lorenzo and Müller 2008; Thanh et al. 2014). Kulterer explains this by the fact that the nonsolvent solvation power for CDA in water decreases with increasing temperature, since the water affinity of CDA also decreases with increasing temperature (Bochek and Kalyuzhnaya 2002; Kulterer et al. 2011).

The jump in particle size development in the concentration range between 5 and 10 mg $mL^{-1}$ can be explained using the concept of the critical overlap concentration $c^*$. Therefore, we performed additional measurements to determine $c^*$ by Ubbelohde viscosimetry using a dilution series of CDA in THF (0–15 mg $mL^{-1}$). Subsequently, the specific viscosity was determined and plotted as a function of the concentration, Fig. 8.

This results in an determined value of 9.8 mg $mL^{-1}$ for $c^*$. Below $c^*$ the polymers are in a dispersed state and can be separated into nanodomains resulting in smaller and more uniform particles through precipitation (Hornig and Heinze 2008). At higher concentrations, the hydrodynamic volumes of the polymers overlap, leading to uncontrolled precipitations (Cordt et al. 2020). This corresponds exactly to the increase in mean particle size between 5 and 10 mg $mL^{-1}$.

In general, the results show that the increase of the applied concentration favors the production of polydisperse and larger particles with a bimodal distribution. In contrast, cooling with an IB promotes the formation of smaller and more uniform particles. To the best of our knowledge, there is no report in the literature of bimodal distributions obtained by the selected process parameters. The larger fraction D2 behaves as already described in the literature. The fraction with the smaller particles D1, in turn, shows a different behavior. For a more detailed description of this, further investigations must be carried out. In particular, however, both fractions can be separated from each other by centrifugation or filtration processes and used for specific applications.

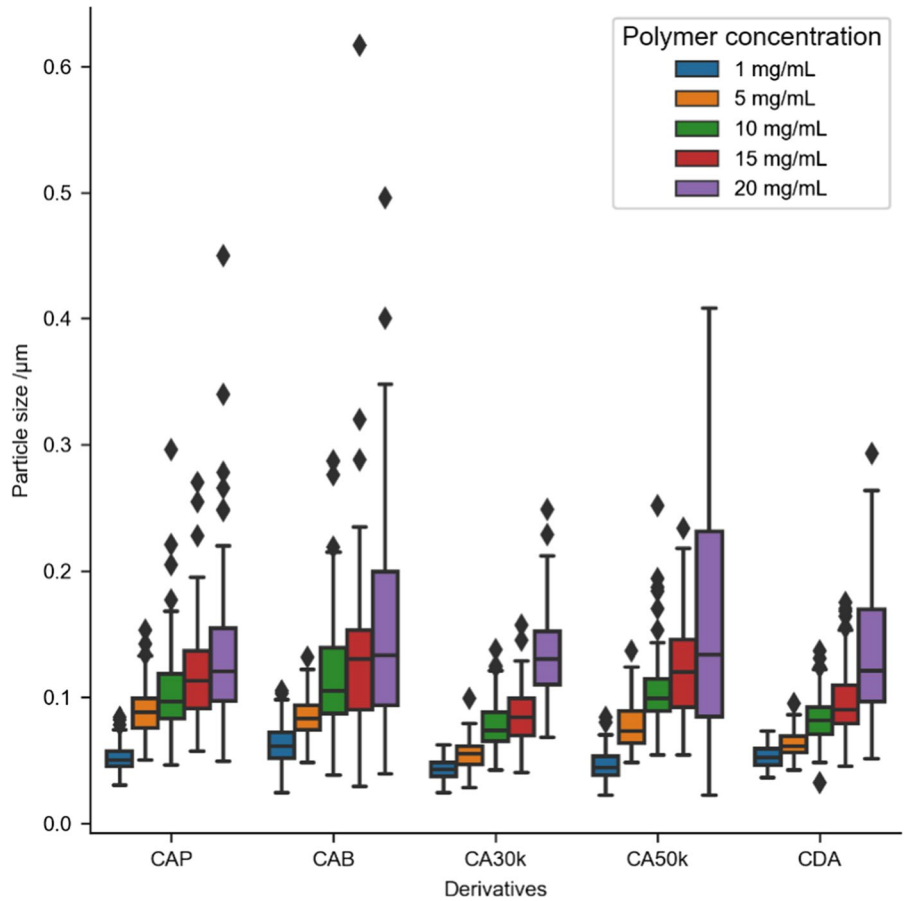


**Fig. 9** Box plot of the particle size distribution for the used cellulose acetate derivatives with different molecular weights and concentrations

*Particle formation via rapid solvent shifting*

For the rapid solvent shifting, the antisolvent was quickly injected into the organic solution, resulting in an accelerated precipitation of the polysaccharide-based nanoparticles (Whittemore IV 2015). For this investigation, various cellulose acetates differing in chain length as well as the cellulose acetate derivatives CAP and CAB were examined. Unimodal size distributions were obtained through the rapid solvent exchange.

As the concentration increases, the average particle diameter increases as well as the respective standard deviation for all samples, Fig. 9. The mean size of the obtained nanoparticles can be adjusted between 43 and 158 nm through the suitable choice of the hydrophobic cellulose ester and the applicable concentration.

The DS from the elemental analysis is 2.0 for CDA and 2.2 for CA30k and CA50k, respectively. It can be seen that the slight difference in DS has no recognizable influence on the particle size distribution.

The molecular weight distributions from the SEC measurements of the individual cellulose acetate derivatives differ slightly from the information provided by the manufacturer, Supplementary Table ST1. In the considered concentration range of the nanoprecipitation, the different molecular weight distributions also had no influence on the particle size. This is in contradiction to a previous report (Kulterer et al. 2011). Only the applied concentration of the respective derivatives has an influence on the resulting particle sizes. A linear regression of the concentration x versus the average particle sizes y yields the function $y = 0.0046x + 0.0479$ with $R^2 = 0.989$. This offers the possibility to estimate a desired average particle size depending on the selected polymer concentration. The smallest and most uniform nanoparticles were produced at a concentration of 1 mg $mL^{-1}$.

Despite the strong variation of the chain lengths, similar particle sizes for the different cellulose acetate derivatives were obtained from highly diluted solutions. However, CAP and CAB show a stronger tendency to form larger particles in contrast to the shorter chain length in cellulose acetate derivatives as already reported (Hornig and Heinze 2008). This could possibly be explained by the larger side chains after functionalization. The preparation of CAP nanoparticles has caused a slight degradation of the molecular weight as a result of the applied shear forces. It should also be mentioned that due to the rapid solvent exchange, the sudden increase in particle size between 5 and 10 mg $mL^{-1}$ can no longer be detected in any of the samples.

The chain length of the cellulose acetate derivatives has a rather minor influence on the morphology of the obtained particles. The cellulose acetates with different molecular weights result in predominantly smooth and rough spherical particles, whereas the use of CAP and CAB makes it possible to produce almost exclusively smooth and perfectly spherical particles. From this, the tendency can be seen that the side chains have a stronger influence on the morphology and the mean particle size of the resulting particles than the molecular weights of the used polymers. Due to the rapid solvent shifting, the jump in the particle size between 5 and 10 mg $mL^{-1}$ is no longer clearly recognizable, so that the c* shows a minor influence here.

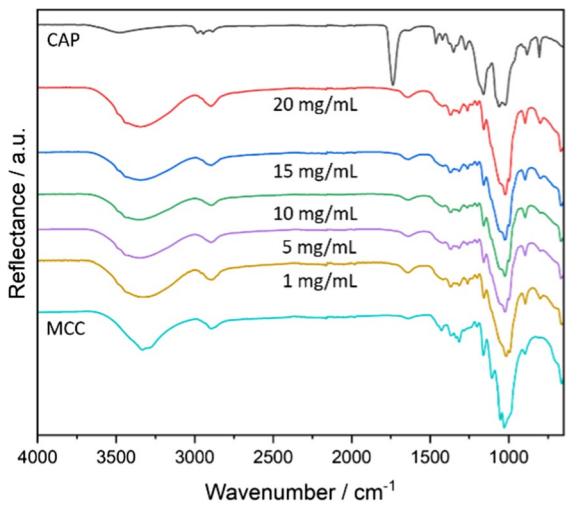


**Fig. 10** FTIR spectra of CAP particles, the deacetylated CAP nano- and submicroparticles produced through the concentration range of 1, 5, 10, 15 and 20 mg $mL^{-1}$ and MCC.

## Fabrication of cellulose nano- and submicronparticles

For the production of cellulose particles, two ways are presented. One way is to prepare these from cellulose acetate derivative particles via simple deacetylation (1). The other route is to obtain nanoparticles directly from cellulose by dissolving MCC and precipitating and regenerating it via the rapid solvent shifting method (2).

Process (1) is illustrated using CAP particles as an example. Here, the particles of the entire concentration series are each deacetylated by a 0.15 M NaOH in a 96 vol% ethanol solution. This should completely remove both the acetyl and propionyl residue. This can be achieved using either an aqueous or an alcoholic alkali solution. The degree of deacetylation and the time required depend on many factors, such as the solvent type, alkali concentration and the applied ratio (He 2017; Tulos et al. 2019). According to Liu and Hsieh, the deacetylation of cellulose acetate with an alcoholic alkali solution should be more efficient, homogeneous and complete than with the same alkali concentration in an aqueous solution (Liu and Hsieh 2002). In addition, there should be no significant change in surface and morphology. In order to perform a complete deacetylation, the reaction was carried out for 24 h at RT. Subsequently, FTIR was used to characterize the deacetylation results, Fig. 10.

FTIR analysis was performed on CAP particles and the deacetylated samples in the concentration range from 1 mg $mL^{-1}$ to 20 mg $mL^{-1}$ and MCC. This makes it possible to detect the complete deacetylation of the specimens. The FTIR spectra of CAP particles show the typical spectrum of CAP. Most notable is the small band at 2886 $cm^{-1}$ for the methylene group ($–CH_2$-) of the propionyl moiety and the strong absorption band at 1739 $cm^{-1}$ which is related to the carbonyl (C=O) stretching vibration (Xu et al. 2018; Rothammer et al. 2018). The respective deacetylation leads to the formation of free hydroxyl groups and thus to a strong increase of the band around 3345 $cm^{-1}$. These can be assigned to the valence vibrations of the hydroxyl groups within the cellulose chains as well as to the vibrations of absorbed water. They include signals from inter- and intramolecular interactions between the

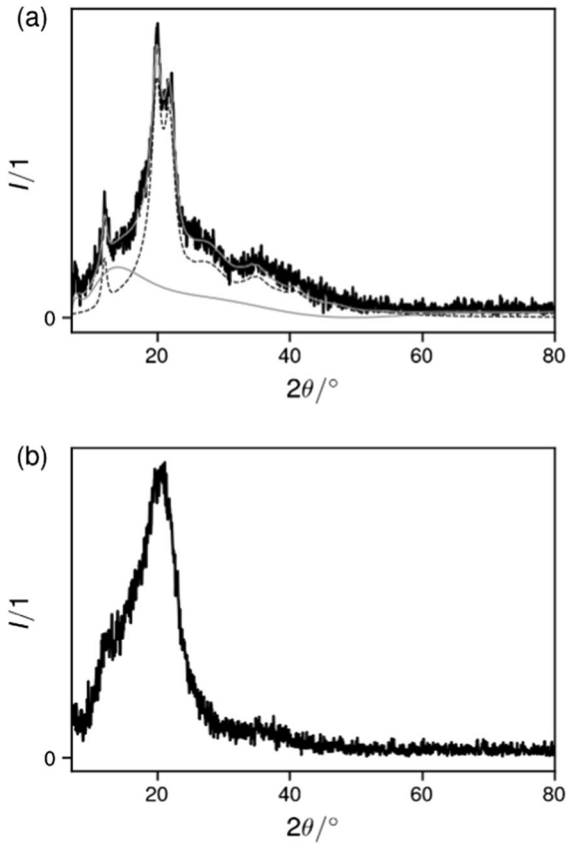


**Fig. 11** Diffraction patterns of **a** deacetylated CAP nanoparticle sample (method 1) and **b** cellulose nanoparticle sample (method 2). The presented data were smoothed over 5 data points (spaced by 0.02° 2θ) by a Savitzky-Golay algorithm and corrected for scattering from the sample holder. In **a**, the pattern is explained as the sum of coherent (dashed line) and incoherent scattering (gray line), the latter being composed of scattering from the amorphous phase and diffuse scattering from the crystalline phase

molecular chains (Ciolacu et al. 2011). In the range between 2800 cm and 3000 $cm^{-1}$ are the valence vibrations of the alkyl groups. Here, a clear change from small bands around 2886 $cm^{-1}$ of CAP can be seen. The strong band of carbonyl stretching vibration vanished in all treated samples indicating complete deacetylation. A further band of absorbed water is located at 1635 $cm^{-1}$. The band in the region around 1429 $cm^{-1}$, which is partially recognizable as a shoulder, can be assigned to symmetrical deformation vibrations of the $CH_2$ groups of the cellulose. In the region between 1000 cm and 1300 $cm^{-1}$ the bands of the C–O valence vibrations of the alcohol groups and

**Table 2** Calculated crystallinity of MCC and cellulose particles prepared via method (1) in the concentration range of 1, 5, 10, 15 and 20 mg $mL^{-1}$

| Substance | Crystallinity/% |
|---|---|
| MCC | 60.42 ± 0.14 |
| 1 mg/mL | 37.90 ± 0.31 |
| 5 mg/mL | 37.95 ± 0.10 |
| 10 mg/mL | 30.60 ± 0.11 |
| 15 mg/mL | 36.27 ± 0.10 |
| 20 mg/mL | 38.62 ± 0.39 |

the pyran ring are located. Around 897 $cm^{-1}$ are the stretching vibrations of the glycosidic bonds. Thus, the spectra of the deacetylated samples correspond well to the spectrum of the MCC. The deacetylation has therefore led to a complete conversion of the CAP to cellulose.

Subsequently, the cellulose nanoparticles obtained via methods 1 and 2 were further characterized via X-ray diffraction, Fig. 11. For each of the produced regenerated cellulose particles, the main intensity contributions are at 12.02°, 20.12° and 22.20°. The peak at 12.02° corresponds to the Miller index of (1–10). The broad peak at 20.40° of the cellulose nanoparticles consists of the contributions from two adjacent reflections which are clearly visible in the deacetylated sample. The diffraction pattern at 20.12° and the corresponding shoulder at about 22.20° can be assigned to the Miller indices of (110) and (020).

As a result of this classification, the diffraction pattern of the cellulose regenerates of both approaches corresponds to the cellulose II modification. Here, the cellulose chains have an antiparallel orientation. This represents the thermodynamically more stable modification of cellulose (French 2014).

The crystallinity of the samples was determined according to the method of Ruland and Vonk (Ruland 1961; Vonk 1973). For this, the data were evaluated by a Rietveld refinement. Here, the MCC has a crystallinity of about 60%. By dissolving and regenerating CAP via nanoprecipitation followed by deacetylation, the crystallinity of the obtained cellulose nanoparticles decreases to 31–38%, Table 2. In contrast, the cellulose nanoparticles prepared directly from MCC via method 2 exhibit a completely amorphous structure. Here, MCC exhibits a crystallite size of 8.3 nm. For the obtained particles prepared from a 1 mg

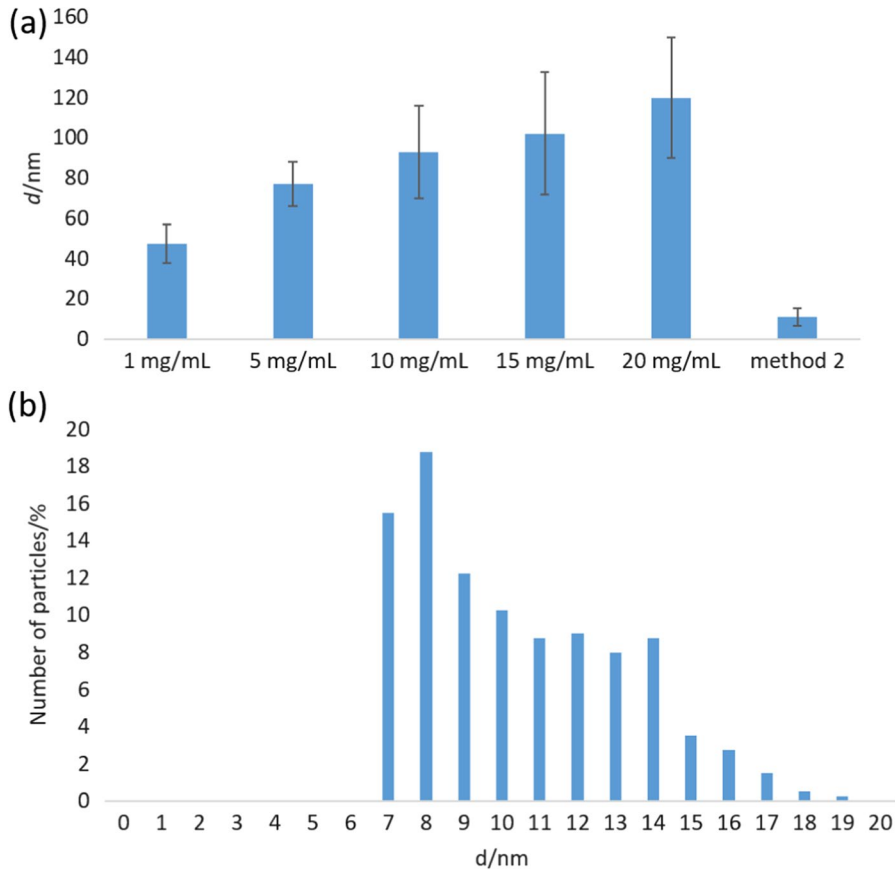


**Fig. 12** **a** Average size of cellulose particles produced via method 1 by using a concentration of 1, 5, 10, 15 and 20 mg $mL^{-1}$ for the nanoprecipitation and by using method 2. **b** Particle size distribution of method (2)

$mL^{-1}$, 5 mg $mL^{-1}$ and 10 mg $mL^{-1}$, the crystallite size reduces to 6.2 nm, 4.4 and 5.5 nm. The particles obtained at concentrations of 15 and 20 mg $mL^{-1}$ have a crystallite size of 4.7 and 5.8 nm.

Since the bands of the FTIR spectra as well as the X-ray diffraction pattern exclusively reflect the chemical structure of cellulose, the complete deacetylation can be considered as successful.

After deacetylation of the CAP particles, the morphological structure of the spheres is preserved in all samples. As the particles have a high surface-to-volume ratio and are characterized by a strong hydrophilicity, strong intermolecular interactions are formed between the spheres. This leads to an increased aggregation of the individual particles. Combined with the high sensitivity of cellulose to electron beam damage, this complicates a suitable imaging of isolated particles (Ogawa and Putaux 2019). Figure 7f shows the cellulose nanoparticles obtained by method (2). Due to their small sizes, highly diluted dispersions in ethanol were studied by TEM, which allows the identification of isolated small circular nanoparticles to be seen. The differences between the mean particle sizes fabricated via methods 1 and 2 are shown in Fig. 12a. Comparing the obtained mean particle sizes of the deacetylated CAP particles with the initial product, a reduction in particle size of about 8.8–13.6% can be observed. The removal of the acetyl and propionyl moieties via an alcoholic alkali solution thus leads to a reduction in particle size while retaining the morphological structure.

For the determination of the size distribution of the nanoparticles produced via method 2, the TEM images were evaluated. The particle diameters were determined via the areas of the separated particles. To avoid possible artefacts, a minimum area was set as a limiting value. Since the unit cell of the anhydroglucose unit requires a volume of 0.671 $nm^3$, a minimum volume of 148.3 $nm^3$ can be assumed for a DP of about 221 units (Barry et al. 1936). Assuming spherical particles, this corresponds to a minimum radius of 3.28 nm and thus a minimum circular area

of 33.8 $nm^2$. Only particles exceeding this limit were included in the particle size distribution. This results in a narrow size distribution in the size range of 7 to 19 nm using method 2. The respective maximum is at 8 nm with a fraction of 18.75%, Fig. 12b. Therefore, both methods show that cellulose nanoparticles can be manufactured via deacetylation of cellulose acetate derivatives and directly via nanoprecipitation starting from a cellulose solution in DMAc/LiCl.

*Comparison of the different manufacturing processes in terms of sustainability*

For the production of particles, the dialysis method is a more sustainable approach. No additional energy input is required due to a missing thermal treatment. The required water can be purified and reused after dialysis if necessary. The solvent displacement method requires an additional energy input due to the use of the syringe pump and the heating up to 73 °C. The rapid solvent shifting is therefore a more sustainable approach, since the syringe pump is not required due to the direct and complete addition of the coagulation medium. For the production of particles directly from cellulose, it is necessary to dissolve it. The process shown here represents an already improved procedure compared to Rahn et al. (1996). Nevertheless, a temperature of 90 °C is required. An optimization of the process by improving the pre-activation could further reduce the required temperature. This would also counteract the known yellowing of the cellulose and make the process more efficient in terms of energy consumption.

However, the solvents acetone, DMAc and THF used in the approaches are not harmless to humans or the environment. The solvents can form explosive air mixtures. The substances cause irritation in each case. Acetone additionally causes drowsiness, DMAc is suspected to have a reproductive toxic and teratogenic effect and THF is carcinogenic (Sigma-Aldrich- SIGALD- 179124, 2023; Sigma-Aldrich-Aldrich- 185,884, 2023; Sigma-Aldrich- Sigma-Aldrich- 401,757, 2023).

The individual methods exhibit advantages and disadvantages depending on the duration of the individual process and the chemicals used. In general, it is essential in terms of sustainability and green chemistry to find and use environmentally friendly alternative solvent systems.

## Conclusion

A comparative study of the production of particles by different types of nanoprecipitation using a wide range of substrates was performed. It has been shown that the difference in dielectric constants $\Delta\epsilon$ of the solvent/antisolvent pair has an influence on the morphology of the produced cellulose-based particles. Variations in the particle size distribution of different nanoprecipitation methods have been highlighted. A fast addition of the coagulation medium under cooling of the batch results in small diameters with narrower size distribution in dependence of the polymer concentration. The particle size distribution seems to be independent of the molecular weight of the polymer used for particle fabrication. The average particle size and the width of distribution rises with a higher polymer concentration during particle formation. Two routes were demonstrated for the manufacturing of nanoscale cellulose spheres. First, cellulose nanoparticles can be obtained via a simple deacetylation of the produced cellulose acetate derivative nanoparticles. Second, cellulose can also be converted into particles in the size range of $10 \pm 3$ nm directly from solution via nanoprecipitation by the rapid solvent shifting process.

**Acknowledgments** The authors thank Eda Duranay for her support in the lab.

**Author contributions** Conceptualization: MRe. Data curation: MRe, FE, and MRo. Formal analysis: MRe, FE, and MRo. Investigation: MRe, FE, MRo, DVO. Methodology: MRe, FE, MRo, and DVO. Supervision: DVO and CZ. Writing: MRe, FE, and MRo.

**Funding** Open Access funding enabled and organized by Projekt DEAL. This work was supported by the Bavarian State Ministry of the Environment and Consumer Pro-tection through financing the collaborational project “BayBionik”.

**Data availability** The data used during this study is available and can be presented upon request.

**Declarations**

**Conflict of interest** The authors declare no competing interests.

**Ethical approval** Not applicable.

**Consent for publication** All authors consent for this publication if approved.



## References

Sigma-Aldrich-Aldrich-185884, Safety data sheet according to Regulation (EC) No. 1907/2006, *N*,*N*-Dimethylacetamide, Version 6.7, Revision Date: 18.03.23, Print Date: 04.04.23. https://www.sigmaaldrich.com/DE/en/sds/aldrich/185884

Aschenbrenner E, Bley K, Koynov K, Makowski M, Kappl M, Landfester K, Weiss CK (2013) Using the polymeric ouzo effect for the preparation of polysaccharde-based nanoparticles. Langmuir 29:8845–8855. https://doi.org/10.1021/la4017867

Bakshi MS, Singh J, Kaur H, Ahmad ST, Kaur G (1996) Thermodynamic behavior of mixtures: 3: mixtures of acetonitrile with dimethylacetamide, dimethyl sulfoxide, nitrobenzene, and methanol at 25°C. J Chem Eng Data 41:1459–1461. https://doi.org/10.1021/je960180l

Barreras-Urbina CG, Ramírez-Wong B, López-Ahumada GA, Burruel-Ibarra SE, Martínez-Cruz O, Tapia-Hernández JA, Félix FR (2016) Nano- and micro-particles by Nanoprecipitation: possible application in the food and agricultural industries. Int J Food Prop 19:1912–1923. https://doi.org/10.1080/10942912.2015.1089279

Barry AJ, Peterson FC, King AJ (1936) X-ray studies of reactions of cellulose in non-aqueous systems: i: interaction of cellulose and liquid ammonia. J Am Chem Soc 58:333–337. https://doi.org/10.1021/ja01293a043

Beaumont M, Nypelö T, König J, Zirbs R, Opietnik M, Potthast A, Rosenau T (2016) Synthesis of redispersible spherical cellulose II nanoparticles decorated with carboxylate groups. Green Chem 18:1465. https://doi.org/10.1039/C5GC03031E

Beaumont M, Rosenfeldt S, Tardy BL, Gusenbauer C, Khakalo A, Nonappa, Opietnik M, Potthast A, Rojas OJ, Rosenau T (2019) Soft cellulose II nanospheres: sol-gel behavior swelling and material synthesis. Nanoscale 11:17773. https://doi.org/10.1039/C9NR05309C

Bergmann J, Kleeberg R, Taut T, Haase A (1998) Quantitative phase analysis using a new Rietveld algorithm - assisted by improved stability and convergence behavior. Advances in X-Ray Analysis 40:422–432

Bochek AM, Kalyuzhnaya LM (2002) Interaction of Water with Cellulose and Cellulose Acetates as influenced by the Hydrogen Bond System and hydrophilic-hydrophobic balance of the macromolecules. Russ J Appl Chem 75:989–993. https://doi.org/10.1023/A:1020309418203

Carrick C, Wågberg L, Larsson PA (2014) Immunoselective cellulose nano-spheres: a versatile platform for nanotheranostics. ACS Macro Lett 3:1117–1120. https://doi.org/10.1021/mz500507k

Carvalho JPF, Silva ACQ, Silvestre AJD, Freire CSR, Vilela C (2021) Spherical cellulose micro and nanoparticles: a review of recent developments and applications. Nanomaterials 10:2744. https://doi.org/10.3390/nano11102744

Chen XQ, Deng XY, Shen WH, Jia MY (2018) Preparation and characterization of the spherical nanosized cellulose by the enzymatic hydrolysis of pulp fibers. Carbohydr Polym 181:879–884. https://doi.org/10.1016/j.carbpol.2017.11.064

Chronopoulou L, Fratoddi I, Palocci C, Venditti I, Russo MV (2009) Osmosis based method drives the self-assembly of polymeric chains into micro- and nanostructures. Langmuir 25:11940–11946. https://doi.org/10.1021/la9016382

Ciolacu D, Ciolacu F, Popa VI (2011) Amorphous cellulose: structure and characterization. Cellulose Chem Technol 45:13–21

Cordt C, Meckel T, Geissler A, Biesalski M (2020) Entrapment of hydrophobic biocides into cellulose acetate nanoparticles by Nanoprecipitation. Nanomaterials 10:2447. https://doi.org/10.3390/nano10122447

Cui Y, Zhang H, Wang J (2022) Preparation of ethyl cellulose particles with different morphologies through microfluidics. Soft Matter 18:1455–1462. https://doi.org/10.1039/D1SM01706C

El-Wakil NA, Hassan ML (2008) Structural changes of regenerated cellulose dissolved in FeTNa, NaOH/thiourea, and NMMO systems. J Appl Polym Sci 109:2862–2871. https://doi.org/10.1002/app.28351

Fessi H, Puisieux F, Devissaguet JP, Ammoury N, Benita S (1989) Nanocapsule formation by interfacial polymer deposition following solvent displacement. Int J Pharm 55:R1–R4. https://doi.org/10.1016/0378-5173(89)90281-0

Feynman RP (1960) There's plenty of room at the bottom. Eng Sci 23:22–36

French AD (2014) Idealized powder diffraction patterns for cellulose polymorphs. Cellulose 21:885–896. https://doi.org/10.1007/s10570-013-0030-4

He X (2017) Optimization of Deacetylation process for regenerated hollow fiber membranes. Int J Polym Sci 2017:3125413. https://doi.org/10.1155/2017/3125413

Heinze T, Koschella A (2005) Solvents applied in the field of cellulose chemistry: a mini review. Polimeros 15:84–90. https://doi.org/10.1590/S0104-14282005000200005

Hornig S, Heinze T (2008) Efficient Approach to design stable water-dispersible nanoparticles of hydrophobic cellulose esters. Biomacromolecules 9:1487–1492. https://doi.org/10.1021/bm8000155

Kannan SK, Duraisamy D, Sudhakar Y (2018) Nanoprecipitation as emerging technique for nanosuspension in ocular delivery: a review. Int J Curr Res 10:64131–64141 (**ISSN: 0975-833X**)

Kulterer MR, Reischl M, Reichel V, Hribernik S, Wu M, Köstler S, Kargl R, Ribitsch V (2011) Nanoprecipitation of cellulose acetate using solvent/nonsolvent mixtures as dispersive media. Colloids Surf 375:23–29. https://doi.org/10.1016/j.colsurfa.2010.11.029

Kumari S, Ram B, Kumar D, Ranote S, Chauhan GS (2018) Nanoparticles of oxidized-cellulose synthesized by green method. Mater Sci Technol 1:22–28. https://doi.org/10.1016/j.mset.2018.04.003

Liu H, Hsieh HL (2002) Ultrafine Fibrous cellulose membranes from electrospinning of cellulose acetate. J Polym Sci Part B Polym Phys 40:2119–2129. https://doi.org/10.1002/polb.10261

Lorenzo AT, Müller AJ (2008) Estimation of the nucleation and crystal growth contributions to the overall crystallization energy barrier. J Polym Sci B Polym Phys 46:1478–1487. https://doi.org/10.1002/polb.21483

Luzi F, Torre L, Kenny JM, Puglia D (2019) Bio- and fossil-based polymeric blends and nanocomposites for packaging: structure–property relationship. Materials 12:471. https://doi.org/10.3390/ma12030471

Mohan T, Ajdnik U, Nagaraj C, Lackner F, Štiglic AD, Palani T, Amornkitbamrung L, Gradišnik L, Maver U, Kargl R, Kleinschek KS (2022) One-step fabrication of hollow spherical cellulose beads: application in pH-responsive therapeutic delivery. ACS Appl Mater Interfaces 14:3726–3739. https://doi.org/10.1021/acsami.1c19577

Ogawa Y, Putaux JL (2019) Transmission electron microscopy of cellulose: part 2: technical and practical aspects. Cellulose 26:17–34. https://doi.org/10.1007/s10570-018-2075-x

Parker RM, Zhao TH, Frka-Petesic B, Vignolini S (2022) Cellulose photonic pigments. Nat Commun 13:3378. https://doi.org/10.1038/s41467-022-31079-9

Raghav N, Sharma MR, Kennedy JF (2021) Nanocellulose: a mini-review on types and use in drug delivery systems. Carbohydr Polym Technol Appl 2:100031. https://doi.org/10.1016/j.carpta.2020.100031

Rahn K, Diamantoglou M, Klemm D, Berghmans H, Heinze T (1996) Homogeneous synthesis of cellulose p-toluenesulfonates in *N*,*N*-dimethylacetamide/LiCl solvent system. Angew Makromol Chem 238:143–163. https://doi.org/10.1002/apmc.1996.052380113

Reimer M, Van Opdenbosch D, Zollfrank C (2021) Fabrication of cellulose-based biopolymer optical fibers and their theoretical attenuation limit. Biomacromolecules 22:3297–3312. https://doi.org/10.1021/acs.biomac.1c00398

Rothammer M, Heep MC, von Freymann G, Zollfrank C (2018) Enabling direct laser writing of cellulose-based submicron architectures. Cellulose 25:6031–6039. https://doi.org/10.1007/s10570-018-2002-1

Rothammer M, Meiers DT, Maier M, von Freymann G, Zollfrank C (2023) Initiator-free photo-cosslinkable cellulose-based resists for fabricating submicron patterns via direct laser writing. J Opt Soc Am B 40:849–855. https://doi.org/10.1364/JOSAB.47965

Ruland W (1961) X-ray determination of crystallinity and diffuse disorder scattering. Acta Crystallogr 14:1180–1185. https://doi.org/10.1107/S0365110X61003429

Schulze P (2016) Incorporation of hydrophobic dyes within cellulose acetate and acetate phthalate based nanoparticles. Macromol Chem Phys 217:1823–1833. https://doi.org/10.1002/macp.201600160

Sigma-Aldrich-SIGALD-179124, Safety data sheet according to Regulation (EC) No. 1907/2006, Acetone, Version 6.10, Revision Date: 21.03.23. https://www.sigmaaldrich.com/DE/en/sds/sigald/179124

Sirviö JA (2019) Fabrication of regenerated cellulose nanoparticles by mechanical disintegration of cellulose after dissolution and regeneration from a deep eutectic solvent. J Mater Chem A 7:755–763. https://doi.org/10.1039/C8TA09959F

Sigma-Aldrich-Sigma-Aldrich-401757, Safety data sheet accorind to Regulation (EC) No. 1907/2006, Tetrahydrofuran, Version 8.10, Revision Date: 29.03.23, Print Date: 04.04.23. https://www.sigmaaldrich.com/DE/en/sds/SIAL/401757

Solin K, Beaumont M, Rosenfeldt S, Orelma H, Borghei M, Bacher M, Opietnik M, Rojas OJ (2020) Self-assembly of soft cellulose nanospheres into colloidal gel layers with enhanced protein adsorption capability for next-generation immunoassays. Small 16:2004702. https://doi.org/10.1002/smll.202004702

Sternling CV, Scriven LE (1959) Interfacial turbulence: hydrodynamic instability and the marangoni effect. AIChE J 5:514–523. https://doi.org/10.1002/aic.690050421

Szczęch M, Szczepanowicz K (2020) Polymeric Core-Shell Nanoparticles prepared by spontaneous emulsification solvent evaporation and functionalized by the layer-by-layer method. Nanomaterials 10:496. https://doi.org/10.3390/nano10030496

Terna AD, Elemike EE, Mbonu JI, Osafile OE, Ezeani RO (2021) The future of semiconductors nanoparticles: synthesis, properties and applications. Mater Sci Eng B 272:115363. https://doi.org/10.1016/j.mseb.2021.115363

Thanh NTK, Maclean N, Mahiddine S (2014) Mechanisms of nucleation and growth of nanoparticles in solution. Chem Rev 114:7610–7630. https://doi.org/10.1021/cr400544s

Tulos N, Harbottle D, Hebden A, Goswami P, Blackburn RS (2019) Kinetic analysis of cellulose acetate/cellulose II hybrid fiber formation by alkaline hydrolysis. ACS Omega 4:4936–4942. https://doi.org/10.1021/acsomega.9b00159

Vonk CG (1973) Computerization of Ruland's X-ray method for determination of the crystallinity in polymers. J Appl Polym Sci 6:148–152. https://doi.org/10.1107/S0021889873008332

Wang S, Lu A, Zhang L (2016) Recent advances in regenerated cellulose materials. Prog Polym Sci 53:169. https://doi.org/10.1016/j.progpolymsci.2015.07.003

Whittemore IVJH, Jones AT, Mendon SK, Rawlins JW (2015) Investigation of ouzo effect colloid formation via organosilica nanoparticles. Colloid Polym Sci 293:2671–2680. https://doi.org/10.1007/s00396-015-3657-x

Wondraczek H, Petzold-Welcke K, Fardim P, Heinze T (2013) Nanoparticles from conventional cellulose esters: evaluation of preparation methods. Cellulose 20:751–760. https://doi.org/10.1007/s10570-013-9874-x

Xu Q, Song L, Zhang L, Hu G, Chen Q, Liu E, Liu Y, Zheng Q, Xie H, Li N (2018) Synthesis of cellulose acetate propionate and cellulose acetate butyrate in a $CO_2$/DBU/DMSO system. Cellulose 25:205–216. https://doi.org/10.1007/s10570-017-1539-8

Yao W, Weng Y, Catchmark JM (2020) Improved cellulose X-ray diffraction analysis using Fourier series modeling. Cellulose 27(10):5563–5579

Yeap EWQ, Ng DZL, Prhashanna A, Somasundar A, Acevedo AJ, Xu Q, Salahioglu F, Garland MV, Khan SA (2017) Bottom-up structural design of crystalline drug-excipient composite microparticles via microfluidic droplet-based processing. Cryst Growth Des 17:3030–3039. https://doi.org/10.1021/acs.cgd.6b01701

Yu HY, Zhang H, Song ML, Zhou Y, Yao J, Ni QQ (2017) From Cellulose nanospheres, nanorods to nanofibers: various aspect ratio induced nucleation/reinforcing effects on polylactic acid for robust-barrier food packaging ACS. Appl Mater Interfaces 9:43920–43938. https://doi.org/10.1021/acsami.7b09102

Zhang C, Zhai T, Turng LS (2017) Aerogel microspheres based on cellulose nanofibrils as potential cell culture scaffolds. Cellulose 24:2791–2799. https://doi.org/10.1007/s10570-017-1295-9

Zhang S, Zhang F, Jin L, Liu B, Mao Y, Liu Y, Huang J (2019) Preparation of spherical nanocellulose from waste paper by aqueous NAOH/thiourea. Cellulose 26:5177–5185. https://doi.org/10.1007/s10570-019-02434-9

Zhao XF, Winter WT (2015) Cellulose/cellulose-based nanospheres: perspectives and prospective. Ind Biotechnol 11:34–43. https://doi.org/10.1089/ind.2014.0030

Zielińska A, Carreiró F, Oliveira AM, Neves A, Pires B, Venkatesh DN, Durazzo A, Lucarini M, Eder P, Silva AM, Santini A, Souto EB (2020) Polymeric nanoparticles: production, characterization, toxicology and ecotoxicology. Molecules 25:3731. https://doi.org/10.3390/molecules25163731